

# How Much do Hardware Imperfections Affect the Performance of Reconfigurable Intelligent Surface-Assisted Systems?

ALEXANDROS-APOSTOLOS A. BOULOGEORGOS<sup>1</sup> (Senior Member, IEEE),  
AND ANGELIKI ALEXIOU<sup>1</sup> (Member, IEEE)

Department of Digital Systems, University of Piraeus, 18534 Piraeus, Greece

CORRESPONDING AUTHOR: A.-A. A. BOULOGEORGOS (e-mail: al.boulogeorgos@ieee.org)

This work was supported from the European Commission's Horizon 2020 Research and Innovation Programme under Grant 871464 (ARIADNE).

**ABSTRACT** In the present work, we investigate the impact of transceiver hardware imperfection on reconfigurable intelligent surface (RIS)-assisted wireless systems. In this direction, first, we present a general model that accommodates the impact of the transmitter (TX) and receiver (RX) radio frequency impairments. Next, we derive novel closed-form expressions for the instantaneous end-to-end signal-to-noise-plus-distortion-ratio (SNDR). Building upon these expressions, we extract an exact closed-form expression for the system's outage probability, which allows us not only to quantify RIS-assisted systems' outage performance but also reveals that the maximum allowed spectral efficiency of the transmission scheme is limited by the levels of the transceiver hardware imperfection. Likewise, a diversity analysis is provided. Moreover, in order to characterize the capacity of RIS-assisted systems, we report a new upper-bound for the ergodic capacity, which takes into account the number of the RIS's reflective units (RUs), the level of TX and RX hardware imperfection, as well as the transmission signal-to-noise-ratio (SNR). Finally, two insightful ergodic capacity ceilings are extracted for the high-SNR and high-RUs regimes. Our results highlight the importance of accurately modeling the transceiver hardware imperfection and reveals that they significantly limit the RIS-assisted wireless system performance.

**INDEX TERMS** Diversity order, ergodic capacity, outage probability, performance analysis, reconfigurable intelligent surfaces.

## I. INTRODUCTION

RECONFIGURABLE intelligent surfaces (RISs) have been recognized as one of the key enablers of the sixth generation networks [1], [2]. Most RIS designs consists of two-dimensional (2D) arrays of reflective units (RUs) that are controlled by at least one micro-controller [3]. Each RU can independently change the phase shift of the electromagnetic signal incident upon it [4]. By providing collaboration capabilities between the RUs through the micro-controller, the implicit randomness of the propagation environment can be exploited in order to create preferable wireless channels [5].

Scanning the technical literature, several research work that studied the performance of RIS-assisted systems [6]–[8], presented comparisons with their predecessors, i.e., relays [9]–[11], and provided optimum information and/or

power transfer policies [12]–[15], can be identified. In particular, in [6], Basar *et al.* provided an upper bound for the symbol error rate (SER) of RIS-assisted systems, assuming that the transmitter (TX)-RIS and RIS-receiver (RX) channels are Rayleigh distributed. Similarly, in [7], the authors presented a bit error rate analysis for RIS-assisted systems that employ non-orthogonal multiple access. Additionally, in [8], Zhang *et al.* presented an approximation for the achievable data rate assuming that both the TX-RIS and RIS-RX channels are independent and Rician distributed. In [9], Renzo *et al.* highlighted the fundamental similarities and differences between RIS and relays. In the same work, simulation results were provided in order to compare RIS with relay-assisted systems in terms of achievable data rate. In [10], the authors compared RIS with decode-and-forward

relays in terms of energy efficiency, while in [11], RIS-assisted systems were compared against the corresponding relay ones in terms of outage probability, symbol error rate, diversity gain and order as well as ergodic capacity, assuming that the transceivers in both RIS- and relay-assisted systems were equipped with ideal RF front-ends. Moreover, in [12], the authors presented an energy efficiency maximization strategy for RIS-assisted wireless systems, whereas, in [13], the authors provided a policy that enables the maximization of the achievable rate by jointly optimizing the transceivers beamforming precoders and the RIS phase shifters. Likewise, in [14], a data rate maximization strategy for RIS-assisted unmanned aerial vehicle networks was reported. Finally, in [15], a simultaneous wireless information and power transfer scheme for RIS-assisted systems was discussed.

All the aforementioned works assumed that the transceivers were equipped with ideal radio frequency (RF) front-ends. However, in practice, transceiver suffers from hardware imperfections, which cause in-phase and quadrature imbalance, phase noise and nonlinearities [16]–[23]. Recognizing the fact that hardware imperfections will be one of the main limitations of the RIS-assisted systems, Zhou *et al.* studied the spectral and energy efficiency of RIS-assisted multiple-input single-output systems in the presence of hardware imperfections and revealed their detrimental impact on the performance of such systems [24]. Similarly, in [25], the authors characterized the asymptotic channel capacity of RIS-assisted systems in which both the TX and RX experience hardware imperfections. Additionally, in [26], the capacity degradation due to hardware imperfections in RIS-assisted systems was bounded. However, in [26], the detrimental effect of fading was neglected. Furthermore, [27] and [28], the authors also studied the capacity performance of RIS-assisted wireless systems in the presence of hardware imperfections, assuming deterministic wireless channels. Finally, no outage or diversity analysis were provided in [26]–[28].

To the best of the authors' knowledge, there is no paper in the technical literature that examines the impact of hardware imperfections on the outage performance of RIS-assisted wireless systems and quantifies its ergodic capacity, under the assumption that both the TX-RIS and RIS-RX links are independent and Rayleigh distributed. Motivated by this, the contribution of this paper is as follows:

- We present a general model to accommodate the impact of transceiver impairments on RIS-assisted systems. This model also takes into account the effect of fading as well as the RIS size.
- Next, we extract the instantaneous signal-to-noise-plus-distortion-ratio (SNDR), and we derive novel closed-form expressions for the outage probability of RIS-assisted wireless systems. These expressions are capable of quantifying the outage performance degradation due to hardware imperfections and reveal that in order to achieve an acceptable outage probability, the

spectral efficiency of the transmission scheme should be constrained by a hardware imperfection-dependent limit. As a benchmark, we revisit the outage probability for the special case in which both the TX and the RX are equipped with ideal RF front-ends. Note that the outage probability for ideal TX and RX was initially presented in [11].

- Moreover, we provide a diversity order analysis that reveals that the diversity order of RIS-assisted wireless systems depends only from the number of RIS's RUs.
- Additionally, we present a low-complexity closed-form upper bound for the ergodic capacity of RIS-assisted wireless systems.
- Finally, ergodic capacity ceilings are extracted for the cases in which the signal-to-noise-ratio (SNR) and/or the number of RIS's RUs tend to infinity.

The rest of the paper is organized as follows: Section II describes the RIS-assisted system model that takes into account the effect of transceiver hardware imperfections. Next, Section III provides the theoretical framework that assess the impact of transceiver hardware imperfections on RIS-assisted wireless systems in terms of outage probability and ergodic capacity. Section IV presents respective numerical results, which verify the analysis, accompanied by insightful discussions and observations. Finally, closing remarks that summarize the current contribution, are reported in Section V.

*Notations:* In what follows, the operators  $\mathbb{E}[\cdot]$ ,  $|\cdot|$ , and  $\Pr(\mathcal{A})$  respectively denote the statistical expectation, the absolute value, and the probability of the event  $\mathcal{A}$ . Moreover,  $\lim_{x \rightarrow z}(f(x))$  returns the limit of  $f(x)$  as  $x$  tends to  $z$ . Additionally,  $\Gamma(\cdot)$ ,  $\Gamma(\cdot, \cdot)$  and  $\gamma(\cdot, \cdot)$  respectively stand for the Gamma [29, eq. (8.310)], upper incomplete Gamma [29, eq. (3.350/3)] and lower incomplete Gamma [29, eq. (3.350/2)] functions. Finally,  $(x)_n$  represents the Pochhammer operator [30, eq. (19)].

## II. SYSTEM MODEL

As illustrated in Fig. 1, we consider a scenario in which a single-antenna TX node communicates with a single-antenna RX node through a RIS, which consists of  $N$  RUs. It is assumed that, due to blockage, no-direct link between TX and RX can be established. The baseband equivalent fading channels between the TX and the  $i$ -th RU,  $h_i$ , and the one between the  $i$ -th RU and RX,  $g_i$ , are assumed to be independent and identical. Moreover, it is assumed that  $|h_i|$  and  $|g_i|$  are Rayleigh distributed with scale parameter being equal to 1. Of note, several prior published contributions employ this assumption [6], [8], [11], [12], which originates from the fact that even if the line-of-sight links between the TX and RIS as well as RIS and RX are blocked, there still exist extensive scatters.

The hardware imperfections at the TX cause a mismatch between the intended transmitted signal,  $s$ , and what is actually generated. As a result, the actual transmitted signal can

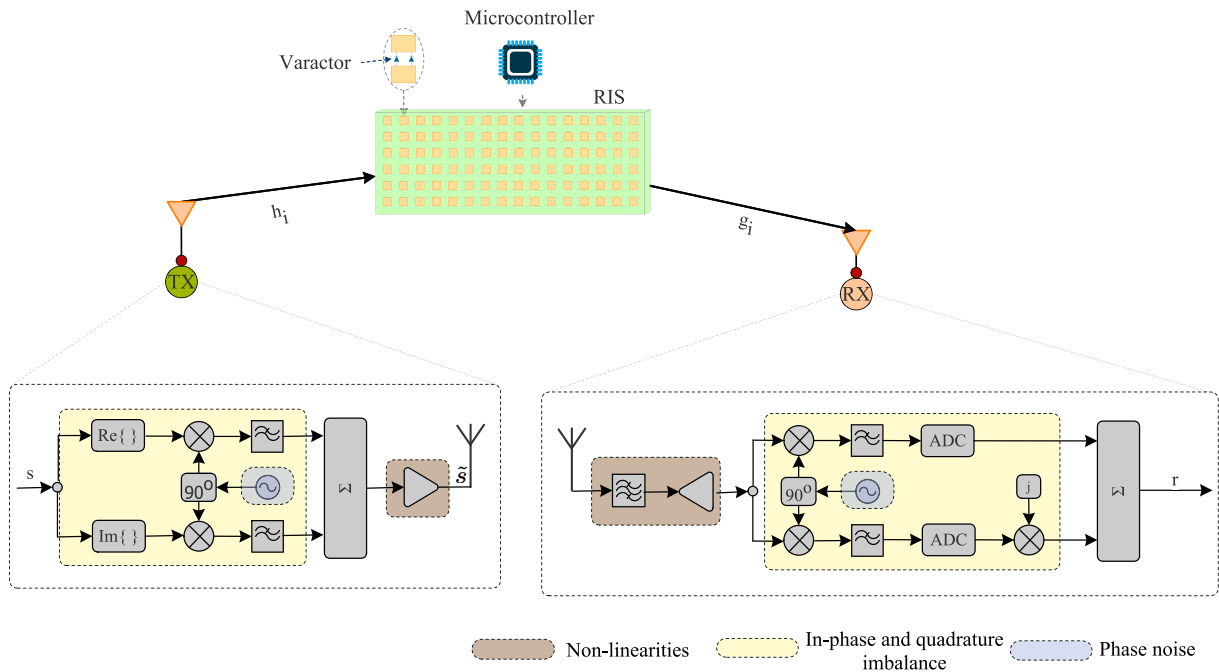


FIGURE 1. System model of the RIS-assisted wireless system. Note that in this figure  $\tilde{s}$  represents the baseband equivalent of the transmitted signal.

be described as

$$\tilde{s} = s + n_t, \quad (1)$$

where  $n_t$  represents the distortion from the TX hardware imperfections, and can be modeled as a zero-mean complex Gaussian process with variance

$$\sigma_t^2 = \kappa_t^2 P_s. \quad (2)$$

In (2),  $\kappa_t$  stands for the TX's error vector magnitude (EVM), which is in-general a non-negative design parameter, while  $P_s$  represents the average transmitted power. Of note, according to the third generation partnership project (3GPP) long term evolution advanced (LTE-A), EVM is in the range of [0.07, 0.175] [31]. Moreover, in high frequency systems, such as millimeter wave and THz ones, EVM may even reach 0.3 [32], [33].

At the RX side, the baseband equivalent received signal can be obtained as

$$r = \sum_{i=1}^N h_i g_i p_i \tilde{s} + n_r + n, \quad (3)$$

where  $n_r$  is the distortion from the RX hardware imperfections, and can be modeled as a zero-mean complex Gaussian process with variance

$$\sigma_r^2 = \kappa_r^2 |A|^2 P_s, \quad (4)$$

with

$$A = \sum_{i=1}^N |h_i| |g_i|, \quad (5)$$

being the equivalent TX-RIS-RX channel. In (4),  $\kappa_r$  represents the RX's EVM. Note that this model has been validated by several analytical and experimental prior works, including [21], [34]–[40] and references therein.

Likewise,  $n$  stands for the white Gaussian noise (AWGN) and can be modeled as a zero-mean complex Gaussian process with variance  $N_o$ . Moreover,  $p_i$  represents the  $i$ -th RU response and can be obtained as

$$p_i = |p_i| \exp(j\phi_i), \quad (6)$$

with  $\phi_i$  standing for the phase shift that is applied by the  $i$ -th RU of the RIS. Without loss of generality, we assume that  $|p_i| = 1$ , which is in line with realistic implementations [41]. In the current contribution, we consider a RIS that uses varactor-tuned RUs, capable of configuring their phase shift by adjusting the bias voltage applied to the varactor [42]. Next, by assuming that the RIS has perfect knowledge of the phase of  $h_i$ ,  $\phi_{h_i}$ , and the one  $g_i$ ,  $\phi_{g_i}$ , and selects the optimal phase shifting, i.e.,

$$\phi = -(\phi_{h_i} + \phi_{g_i}), \quad (7)$$

we can simplify (6) as

$$p_i = \exp(-j(\phi_{h_i} + \phi_{g_i})), \quad (8)$$

Next, by applying (8) into (3) and after some mathematical manipulations, the equivalent received signal at the RX can be expressed as [11, eq. (6)]

$$r = A\tilde{s} + n_r + n. \quad (9)$$

Finally, by substituting (1) into (9), the baseband equivalent received signal can be rewritten as

$$r = As + w + n, \quad (10)$$

where

$$w = An_t + n_r, \quad (11)$$

represents the aggregated distortion caused by the TX and RX hardware imperfections.

*Remark 1:* From (11), it becomes evident that for a given channel realization, the aggregated impact of TX and RX hardware imperfections can be modeled via a zero-mean random variable process with variance

$$\sigma_w^2 = |A|^2(\kappa_t^2 + \kappa_r^2)P_s. \quad (12)$$

Interestingly, (12) reveals that as the transmission power increases, the level of distortion due to transceivers hardware imperfections also increases. Finally, note that (10) reduces to the conventional model that neglects the impact of hardware imperfections, for  $\kappa_t = \kappa_r = 0$ . In this case, from (12),  $\sigma_w^2 = 0$ .

### III. PERFORMANCE ANALYSIS

In this section, the theoretical framework that quantifies the impact of transceivers hardware imperfections on the performance of RIS-assisted wireless systems is presented. Specifically, the structure of this section is as follows: Section III-A provides the instantaneous end-to-end SNDR, whereas Section III-B presents a novel closed-form expression for the outage probability. Likewise, Section III-C returns the diversity order of the RIS-assisted wireless system. Finally, Section III-D reports ergodic capacity upper bounds and ceilings, for the cases in which the SNR and/or the number of RIS's RUs tend to infinity.

#### A. SNDR

From (10) and (12), the instantaneous SNDR can be obtained as

$$\rho = \frac{|A|^2 P_s}{(\kappa_t^2 + \kappa_r^2)|A|^2 P_s + N_o}, \quad (13)$$

or equivalently

$$\rho = \frac{|A|^2}{(\kappa_t^2 + \kappa_r^2)|A|^2 + \frac{1}{\rho_s}}, \quad (14)$$

where

$$\rho_s = \frac{P_s}{N_o}, \quad (15)$$

denotes the transmission SNR.

#### B. OUTAGE PROBABILITY

The following theorem returns a closed-form expression for the RIS-assisted wireless system outage probability.

*Theorem 1:* The outage probability of the RIS-assisted wireless system can be obtained as in (16), given at the bottom of the page. In (16),  $\rho_{th}$  is the SNR threshold.

*Proof:* Please refer to Appendix A. ■

Notice that the SNR threshold is connected with the spectral efficiency of the transmission scheme,  $r$ , through

$$r = \log_2(\rho_{th} + 1). \quad (17)$$

*Remark 2:* From (16) and (17), we observe that the outage probability is always 1 for  $r > \log_2(\frac{1}{\kappa_t^2 + \kappa_r^2} + 1)$ . This means that the spectral efficiency of the transmission scheme is limited by the levels of the transceivers hardware imperfections. Finally, note that this result is independent of the fading characteristic of the channel.

*Remark 3:* For the ideal case in which both the TX and RX are hardware imperfection free, i.e.,  $\kappa_t = \kappa_r = 0$ , (16) reduces to

$$P_o^{id} = \frac{\gamma\left(\frac{\pi^2}{16-\pi^2}N, \frac{2\pi}{16-\pi^2}\sqrt{\frac{\rho_{th}}{\rho_s}}\right)}{\Gamma\left(\frac{\pi^2}{16-\pi^2}N\right)}, \quad (18)$$

which is the same as [11, eq. (31)].

$$P_o = \begin{cases} \frac{\gamma\left(\frac{\pi^2}{16-\pi^2}N, \frac{2\pi}{16-\pi^2}\frac{1}{\sqrt{1-(\kappa_t^2 + \kappa_r^2)\rho_{th}}}\sqrt{\frac{\rho_{th}}{\rho_s}}\right)}{\Gamma\left(\frac{\pi^2}{16-\pi^2}N\right)}, & \rho_{th} \leq \frac{1}{\kappa_t^2 + \kappa_r^2} \\ 1, & \text{otherwise,} \end{cases} \quad (16)$$

$$\mathcal{D} = - \lim_{\rho_s \rightarrow \infty} \left( \frac{\log_2\left(\frac{\gamma\left(\frac{\pi^2}{16-\pi^2}N, \frac{2\pi}{16-\pi^2}\frac{1}{\sqrt{1-(\kappa_t^2 + \kappa_r^2)\rho_{th}}}\sqrt{\frac{\rho_{th}}{\rho_s}}\right)}{\Gamma\left(\frac{\pi^2}{16-\pi^2}N\right)}\right)}{\log_2(\rho_s)} \right) \quad (20)$$

### C. DIVERSITY ORDER

The diversity order can be calculated as

$$D = - \lim_{\rho_s \rightarrow \infty} \left( \frac{\log_2(P_o)}{\log_2(\rho_s)} \right), \quad (19)$$

which, with the aid of (16) and by assuming that  $\rho_{th} \leq \frac{1}{\kappa_t^2 + \kappa_r^2}$ , can be rewritten as in (20), given at the bottom of the previous page. After evaluating the limit in (20), we obtain

$$D = \frac{\pi^2}{16 - \pi^2} \frac{N}{2}. \quad (21)$$

Notice that, according to (21), the diversity order only depends on the number of RIS's RUs and not from the level of imperfections.

### D. ERGODIC CAPACITY

In order to characterize the ergodic capacity of RIS-assisted wireless systems, the following theorem provides an upper bound.

*Theorem 2:* The ergodic capacity,  $C$ , of RIS-assisted wireless systems can be upper bounded as

$$C \leq \log_2 \left( 1 + \frac{\left( \frac{16 - \pi^2}{2\pi} \right)^2 \left( \frac{N\pi^2}{16 - \pi^2} \right)_2}{(\kappa_t^2 + \kappa_r^2) \left( \frac{16 - \pi^2}{2\pi} \right)^2 \left( \frac{N\pi^2}{16 - \pi^2} \right)_2 + \frac{1}{\rho_s}} \right), \quad (22)$$

*Proof:* Please refer to Appendix B. ■

The Lemma 1 returns a high-SNR ergodic capacity ceiling, while Lemma 2 provides a high- $N$  ergodic capacity ceiling.

*Lemma 1 (High-SNR and High- $N$  Ergodic Capacity Ceiling):* As the transmission SNR tends to infinity or as the number of RIS's RUs tends to infinity, the ergodic capacity is constrained by

$$\lim_{\rho_s \rightarrow \infty} C = \log_2 \left( 1 + \frac{1}{\kappa_t^2 + \kappa_r^2} \right). \quad (23)$$

*Proof:* For brevity, the proof is given to Appendix C. ■

*Remark 4:* Lemma 1 reveals that the transceiver hardware imperfections cause an ergodic capacity saturation; thus, the performance of high-rate systems is constrained. Moreover, it becomes apparent that in the high-SNR and high- $N$  regimes, the performance of the system is independent from the number of RUs at the RIS and are fully determined by the level of imperfections.

## IV. RESULTS & DISCUSSION

This section aims at verifying the theoretical framework provided in Section III by means of Monte Carlo simulations, assessing the detrimental impact of transceivers hardware imperfections on RIS-assisted wireless systems, and presenting insightful discussions. Unless otherwise stated, in what follows, we use continuous lines and markers to respectively denote theoretical and simulation results. Moreover, we define  $\kappa = \kappa_t = \kappa_r$ .

Figure 2 demonstrates the outage probability as a function of  $\rho_s$  for different values of  $N$  and  $\rho_{th}$ , assuming  $\kappa = 0.1$ .

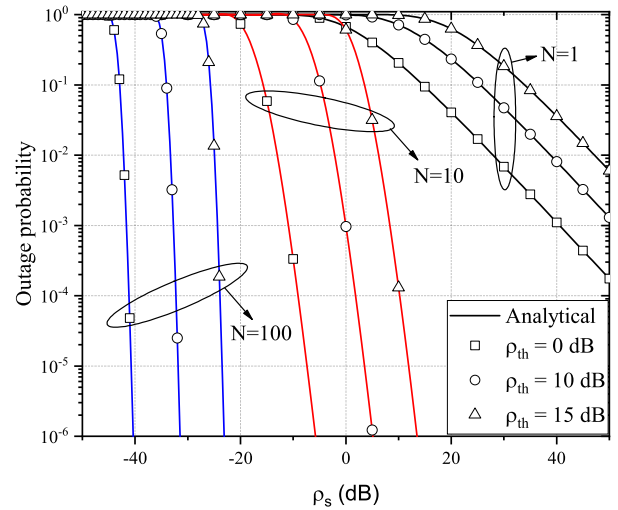


FIGURE 2. Outage probability vs  $\rho_s$  for different values of  $N$  and  $\rho_{th}$ , assuming  $\kappa = 0.1$ .

Of note, according to (17), a  $\rho_{th}$  increase is translated to a spectral efficiency increase. From this figure, we observe that, for fixed  $\rho_{th}$  and  $N$ , as  $\rho_s$  increase, the system's outage performance improves. For example, for  $\rho_{th} = 10$  dB and  $N = 100$ , the outage probability decreases for about 100 times, as  $\rho_s$  increases from  $-33$  to  $-32$  dB. On the other hand, in order to achieve the same outage performance improvement, in a system with  $N = 10$  for the same  $\rho_{th}$ , the transmission SNR should be increased for about 5 dB. This indicates that RIS-assisted systems with higher  $N$  that, based on (21), have higher diversity order, achieve higher diversity gains. In this sense, another way to boost the RIS-assisted system's outage performance, for a given  $\rho_{th}$  and  $\rho_s$ , is to increase  $N$ . For instance, for  $\rho_s = 0$  dB and  $\rho_{th} = 10$  dB, as  $N$  increases from 1 to 10, a 3 orders decrease occurs on the outage probability. Finally, this figures reveals that there exists a trade-off between RIS-assisted system spectral efficiency and power consumption. In more detail, we observe that, for a fixed  $N$  and a predetermined outage probability requirement, in order to increase the system spectral efficiency, i.e., increase  $\rho_{th}$ , the transmission SNR should be also increased; thus, the power consumption would also increase.

Figure 3 depicts the outage probability as a function of the transmission SNR, for different values of  $\rho_{th}$  and  $\kappa$ , assuming  $N = 5$ . As a benchmark, the outage performance for the ideal case in which both the TX and RX does not experience the impact of hardware imperfections, i.e.,  $\kappa = 0$ , is also provided. Moreover, according to 3GPP,  $\kappa = 0.07$  is the lowest achievable EVM for realistic designs, while  $\kappa = 0.2$  is a realistic value for devices operating in high-frequency bands [32], [33]. As expected, we observe that independently of  $\rho_s$  and  $\kappa$ , an outage performance degradation is observed, as  $\rho_{th}$  increases. For instance, for  $\kappa = 0.07$  and  $\rho_s = -5$  dB, the outage probability increases more than 100 times as the

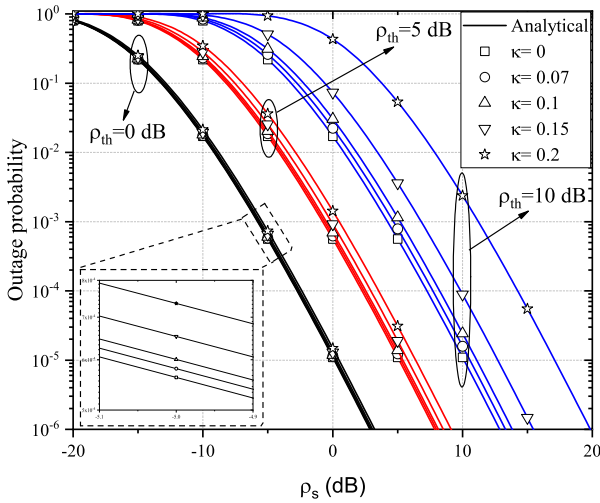


FIGURE 3. Outage probability vs  $\rho_s$ , for different values of  $\rho_{th}$  and  $\kappa$ , assuming  $N = 5$ .

$\rho_{th}$  increases from 0 to 10 dB. Likewise, for given  $\rho_s$  and  $\rho_{th}$ , as  $\kappa$  increases, the outage performance degrades. For example, for  $\rho_s = \rho_{th} = 10$  dB, as  $\kappa$  increases from 0 to 0.15, the outage probability decreases for about 10 times. This indicates the importance of accurately modeling the transceivers' hardware imperfections when assessing the performance of RIS-assisted wireless systems. Moreover, we observe that as  $\rho_{th}$  increases, the impact of hardware imperfections becomes more severe. For instance, for  $\rho_s = -5$  dB and  $\rho_{th} = 0$ , as  $\kappa$  increases from 0 to 0.2, the outage probability increases from 0.017 to 0.021, which is translated into a 23.5% outage performance degradation, while, for the same  $\rho_s$  and for  $\rho_{th} = 10$  dB, the same  $\kappa$  increase results to an outage probability increase for approximately 3 times. Similarly, as  $\rho_s$  increases, the impact of hardware imperfections on the system's outage performance become more detrimental. For example, for  $\rho_{th} = 10$  dB and  $\rho_s = 0$  dB, the outage probability increases for one order of magnitude as  $\kappa$  increases from 0 to 0.2, whereas, for the same  $\rho_{th}$  and  $\rho_s = 10$  dB, the outage probability increases for more than 100 times, as  $\kappa$  increases from 0 to 0.2. To sum up, this figure reveals that there exist a relationship between the transmission SNR, transmission scheme spectral efficiency and level of hardware imperfections, which needs to be taken into account when assessing and designing RIS-assisted wireless systems.

Figure 4 illustrates the impact of hardware imperfections on the outage performance of RIS-assisted systems with different number of RUs. In more detail, the outage probability is plotted as a function of the transmission SNR, for different values of  $N$  and  $\kappa$ , assuming  $\rho_{th} = 10$  dB. Again, as a benchmark, the ideal case in which  $\kappa = 0$  is also depicted. From this figure, it also becomes evident that hardware imperfections have a detrimental impact on the RIS-assisted system performance. In particular, we observe that for a given  $N$ , as  $\kappa$  increases, the transmission SNR

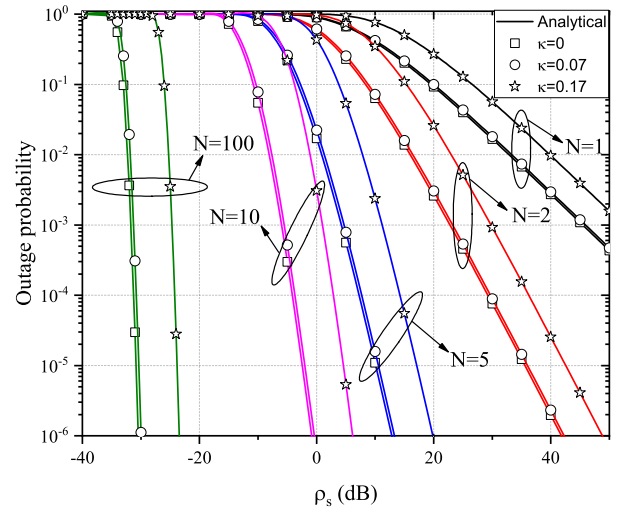


FIGURE 4. Outage probability vs  $\rho_s$ , for different values of  $N$  and  $\kappa$ , assuming  $\rho_{th} = 10$  dB.

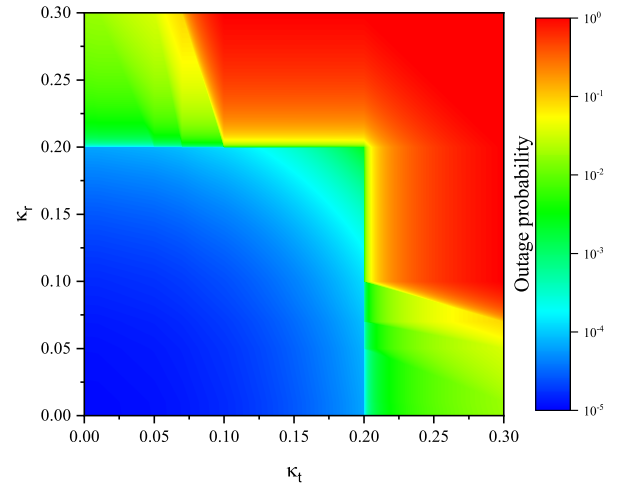


FIGURE 5. Outage probability vs  $\kappa_t$  and  $\kappa_r$ , assuming  $N = 5$ ,  $\rho_s = \rho_{th} = 10$  dB.

should be significantly increase in order for a predetermined outage probability requirement to be satisfied. For instance, for  $N = 100$  and an outage probability requirement of  $10^{-6}$ , the transmission SNR should be increased approximately 6 dB, if  $\kappa$  increases from 0 to 0.17. Similarly, for  $N = 10$  and  $\kappa$  variation, approximately the same transmission SNR increase is required to guarantee a  $10^{-6}$  outage probability requirement. In other words, we observe that the impact of hardware imperfections on the RIS-assisted system outage performance is independent of the number of the RIS's RUs.

Figure 5 demonstrates the outage probability as a function of  $\kappa_t$  and  $\kappa_r$ , assuming  $N = 5$ , and  $\rho_s = \rho_{th} = 10$  dB. From this figure, we observe that, for a given  $\kappa_r$ , as  $\kappa_t$  increases, the outage probability also increases. Similarly, for a fixed  $\kappa_t$ , as  $\kappa_r$  increases, the system outage performance degrades. For example, for  $\kappa_t = 0.1$ , as  $\kappa_r$  increases from 0.1 to 0.2, the outage probability increases from  $2.43 \times 10^{-5}$  to  $1.23 \times 10^{-4}$ . Similarly, for  $\kappa_r = 0.1$ , as  $\kappa_t$  increases from 0.1 to 0.2,

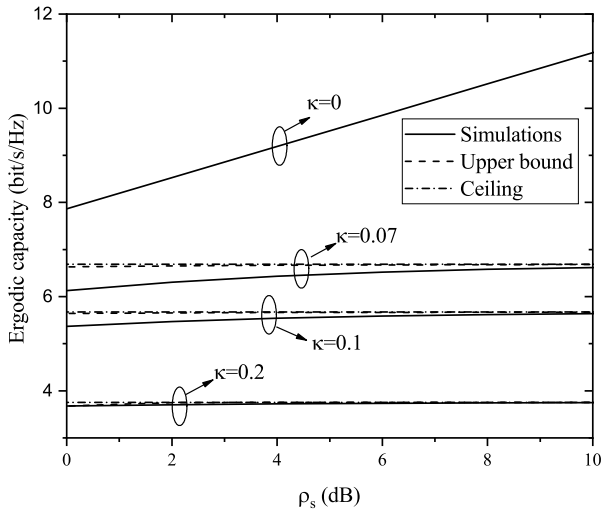


FIGURE 6. Ergodic capacity vs  $\rho_s$ , for different values of  $\kappa$ , assuming  $N = 10$ .

the outage probability also changes from  $2.43 \times 10^{-5}$  to  $1.23 \times 10^{-4}$ . These examples reveal the reciprocal nature of TX and RX hardware imperfections. Finally, it is evident that when the  $\rho_{th} < \frac{1}{\kappa_t^2 + \kappa_r^2}$  is violated, the outage probability becomes equal to 1.

Figure 6 illustrates the impact of transceiver hardware imperfections on the RIS-assisted system ergodic capacity. In more detail, the ergodic capacity is given as a function of  $\rho_s$ , for different values of  $\kappa$ , assuming  $N = 10$ . In this figure, continuous lines are used to denote Monte Carlo simulation results, while for the ergodic capacity upper bound and ceiling dashed and dash-dotted lines employed. As a benchmark, the ideal case in which both the TX and RX are hardware imperfection free, i.e.,  $\kappa = 0$ , is also provided. We observe that for the ideal case, as  $\rho_s$  increases, the ergodic capacity also increases. For example, for a  $\rho_s$  increase from 0 to 10 dB, the ergodic capacity increases from approximately 8 to 11 bits/s/Hz. On the other hand, as described in Lemma 1, in the case of non-ideal transceivers, the ergodic capacity saturates to its ceiling as  $\rho_s$  increases. As a consequence, for a fixed  $\rho_s$ , since the ergodic capacity ceiling is solitary determined by the level of hardware imperfections, i.e.,  $\kappa_t$  and  $\kappa_r$ , both the ergodic capacity and its upper bound as well as the ceiling increase as  $\kappa$  decreases. For example, for  $\rho_s = 5$  dB, as  $\kappa$  decreases from 0.2 to 0.1, the ergodic capacity increases from 3.73 to 5.56 bit/s/Hz, while, for the same  $\kappa$  variation, the upper bound changes from 3.73 to 5.66 and the ceiling from 3.75 to 5.67. This indicates the detrimental effect of hardware imperfections on the system's ergodic capacity. In other words, it highlights the importance of accurately modeling the transceiver hardware imperfections, when assessing the ergodic performance of RIS-assisted systems. Finally, from this figure, it becomes evident that, for practical values of  $\rho_s$ , as  $\kappa$  increases, the upper-bound becomes tighter. As a consequence, for practical values of  $\rho_s$ , the upper bound derived in (22) can

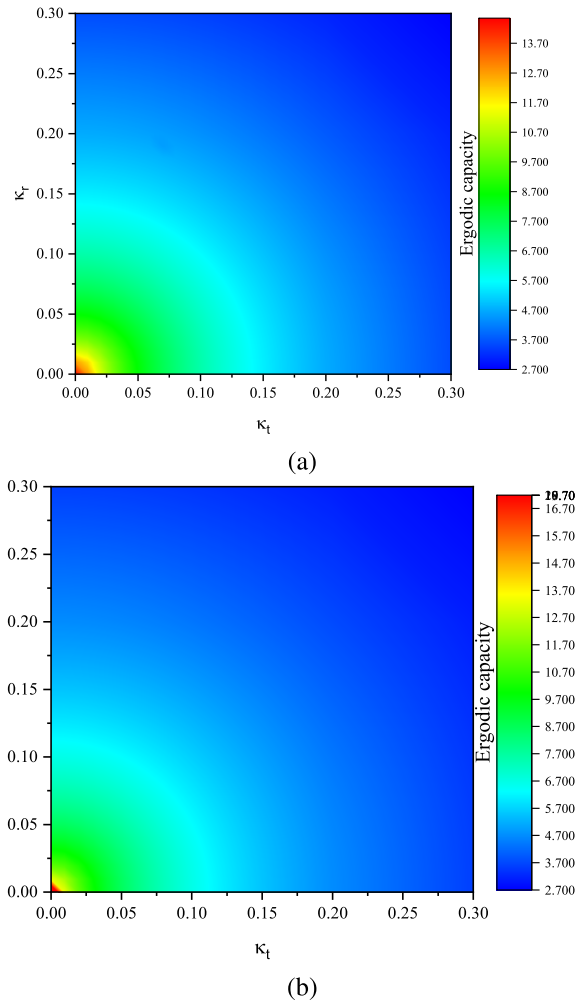


FIGURE 7. Ergodic capacity vs  $\kappa_t$  and  $\kappa_r$ , for (a)  $N = 10$ , (b)  $N = 100$ , assuming  $\rho_s = 20$  dB.

be used as a tight simplified approximation. The accuracy of this approximation increases as the level of hardware imperfections increases.

Figure 7 depicts the ergodic capacity as a function of  $\kappa_t$  and  $\kappa_r$  for different values of  $N$ , assuming  $\rho_s = 20$  dB. In more detail, Fig. 7.a delivers the ergodic capacity for  $N = 10$ , while Fig. 7.b the one for  $N = 100$ . As expected, for given  $\kappa_r$  and  $N$ , as  $\kappa_t$  increases, the level of the hardware imperfections at the TX side increases; hence, the ergodic capacity decreases. For example, for  $\kappa_r = 0.1$  and  $N = 10$ , as  $\kappa_t$  increases from 0.1 to 0.2, the ergodic capacity decreases from 5.67 to 4.39 bit/s/Hz, which corresponds to approximately 22.6% ergodic capacity degradation, whereas, for  $\kappa_r = 0.1$  and  $N = 100$ , the same  $\kappa_t$  change causes the same ergodic capacity degradation. Similarly, for fixed  $\kappa_t$  and  $N$ , as  $\kappa_r$  increases, the ergodic capacity decreases. In more detail, we observe that the reciprocity also holds for the case of ergodic capacity. This mean that regardless of whether the level of hardware imperfections changes in the TX or RX, it will cause the same effect on the RIS-assisted system

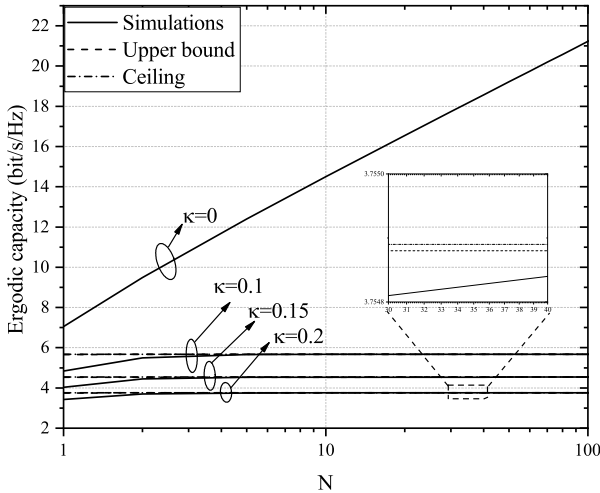


FIGURE 8. Ergodic capacity vs  $N$ , for different values of  $\kappa$ , assuming  $\rho_s = 20$  dB.

ergodic capacity. Finally, by comparing Figs. 7.a and 7.b, we observe that for the case of hardware imperfection-free transceivers, the ergodic capacity significantly increases as  $N$  increases. However, in realistic implementations, the level of hardware imperfections and not the number of the RIS's RUs determines the system's ergodic capacity performance.

In Fig. 8, the ergodic capacity is provided against  $N$ , for different values of  $\kappa$ , assuming  $\rho_s = 20$  dB. For the sake of comparison, the ideal case in which  $\kappa = 0$  is also plotted. From this figure, we observe that in the case in which the transceivers experience the impact of hardware imperfections, as the number of RIS's RUs increases, the ergodic capacity saturates and approaches  $\log_2\left(\frac{1}{\kappa_t^2 + \kappa_r^2}\right)$ . In other words, a specific number of RUs exists beyond which no ergodic capacity gain will be observed as  $N$  increases.

## V. CONCLUSION

In this contribution, we considered a generalized hardware imperfections model, which has been validated in several prior works, in order to assess their impact on RIS-assisted wireless systems. In this direction, we extracted simple closed-form expressions for their outage probability and a novel upper bound for their ergodic capacity, which takes into account the level of transceivers hardware imperfections, the number of RUs at the RIS, as well as the transmission SNR and the spectral efficiency of the transmission scheme. Our results manifested the detrimental impact of transceiver hardware imperfections on the outage and ergodic capacity performance of these systems. In more detail, they revealed that there exists a specific spectral efficiency limit, which solely depends on the level of transceiver hardware imperfections, after with the outage probability becomes 1. Moreover, the importance of accurately modeling the level of transceiver hardware imperfections when evaluating the performance of such systems is reported. Likewise, it is highlighted that there exists a capacity ceiling that is independent of the number of RIS's RUs; however, it is determined by

the TX and RX EVMs. This ceiling cannot be crossed by increasing the transmission SNR or altering the propagation medium characteristics. This is an RIS-assisted wireless system constraint that is expected to influence future designs.

## APPENDIX A PROOF OF THEOREM 1

The outage probability is defined as

$$P_o = \Pr(\rho \leq \rho_{th}), \quad (24)$$

which, by substituting (14), can be rewritten as

$$P_o = \Pr\left(\frac{|A|^2}{(\kappa_t^2 + \kappa_r^2)|A|^2 + \frac{1}{\rho_s}} \leq \rho_{th}\right), \quad (25)$$

or

$$P_o = \Pr\left(|A|^2\left(1 - (\kappa_t^2 + \kappa_r^2)\rho_{th}\right) \leq \frac{\rho_{th}}{\rho_s}\right). \quad (26)$$

For  $1 - (\kappa_t^2 + \kappa_r^2)\rho_{th} \geq 0$ , or equivalently

$$\rho_{th} \leq \frac{1}{\kappa_t^2 + \kappa_r^2}, \quad (27)$$

the outage probability can be written as

$$P_o = \Pr\left(A \leq \frac{1}{\sqrt{1 - (\kappa_t^2 + \kappa_r^2)\rho_{th}}} \sqrt{\frac{\rho_{th}}{\rho_s}}\right), \quad (28)$$

or

$$P_o = F_A\left(\frac{1}{\sqrt{1 - (\kappa_t^2 + \kappa_r^2)\rho_{th}}} \sqrt{\frac{\rho_{th}}{\rho_s}}\right), \quad (29)$$

where  $F_A(\cdot)$  is the cumulative density function (CDF) of  $A$ . Next, by employing [11, eq. (8)], we can obtain the first branch of (16)

For  $1 - (\kappa_t^2 + \kappa_r^2)\rho_{th} < 0$ ,  $|A|^2(1 - (\kappa_t^2 + \kappa_r^2)\rho_{th})$  is always no-positive; hence,  $\Pr(|A|^2(1 - (\kappa_t^2 + \kappa_r^2)\rho_{th}) \leq \frac{\rho_{th}}{\rho_s}) = 1$ , or, based on (26),

$$P_o = 1. \quad (30)$$

## APPENDIX B PROOF OF THEOREM 2

The ergodic capacity can be defined as

$$C = \mathbb{E}[\log_2(1 + \rho)], \quad (31)$$

which can be equivalently written as

$$C = \mathbb{E}\left[\log_2\left(1 + \frac{a}{b}\right)\right], \quad (32)$$

where

$$a = |A|^2, \quad (33)$$

and

$$b = (\kappa_t^2 + \kappa_r^2)|A|^2 + \frac{1}{\rho_s}. \quad (34)$$

We note that the function  $\log_2\left(1 + \frac{a}{(\kappa_t^2 + \kappa_r^2)a + \frac{1}{\rho_s}}\right)$  is concave of  $a$ , for  $a \geq 0$ , since its second derivative is

$$-\frac{1}{\ln(2)} \frac{1}{\rho_s} \frac{2a(\kappa_t^2 + \kappa_r^2)\left(1 + \kappa_t^2 + \kappa_r^2\right) + \frac{1}{\rho_s} + 2\frac{\kappa_t^2 + \kappa_r^2}{\rho_s}}{\left(a(\kappa_t^2 + \kappa_r^2) + \frac{1}{\rho_s}\right)^2} < 0. \quad (35)$$

As a consequence, the Jensen's inequality holds [43], and (32) can be upper-bounded as

$$C \leq \log_2\left(1 + \mathbb{E}\left[\frac{a}{b}\right]\right). \quad (36)$$

However, based on [44, eq. (35)],

$$\log_2\left(1 + \mathbb{E}\left[\frac{a}{b}\right]\right) \approx \log_2\left(1 + \frac{\mathbb{E}[a]}{\mathbb{E}[b]}\right). \quad (37)$$

By combining (36) and (37), we obtain

$$C \leq \log_2\left(1 + \frac{A}{B}\right), \quad (38)$$

where

$$A = \mathbb{E}[a], \quad (39)$$

and

$$B = \mathbb{E}[b]. \quad (40)$$

Of note, the same approach has been employed in several prior works including [44] and references therein.

Next, we provide closed-form expressions for (39) and (40). Based on [45], (39) can be computed as

$$A = \int_0^\infty x^2 f_A(x) dx, \quad (41)$$

where  $f_A(x)$  is the probability density function (PDF) of  $A$ .<sup>1</sup> With the aid of [11, eq. (7)], (41) can be rewritten as

$$A = \frac{1}{\left(\frac{16-\pi^2}{2\pi}\right)^{\frac{N\pi^2}{16-\pi^2}} \Gamma\left(\frac{N\pi^2}{16-\pi^2}\right)} \mathcal{I}, \quad (42)$$

with

$$\mathcal{I} = \int_0^\infty x^{\frac{N\pi^2}{16-\pi^2}+1} \exp\left(-\frac{2\pi}{16-\pi^2}x\right) dx. \quad (43)$$

By setting  $t = \frac{2\pi}{16-\pi^2}$  and then employing [29, eq. (8.310/1)], (43) can be expressed in closed-form as

$$\mathcal{I} = \left(\frac{16-\pi^2}{2\pi}\right)^{\frac{N\pi^2}{16-\pi^2}+2} \Gamma\left(\frac{N\pi^2}{16-\pi^2} + 2\right). \quad (44)$$

1. Note that the PDF, which was provided in [11, eq. (7)] is an extremely tight approximation with an error that is lower than  $10^{-6}$ ; thus, it can be used for the evaluation of the upper bound.

By substituting (44) into (42), we extract

$$A = \left(\frac{16-\pi^2}{2\pi}\right)^2 \frac{\Gamma\left(\frac{N\pi^2}{16-\pi^2} + 2\right)}{\Gamma\left(\frac{N\pi^2}{16-\pi^2}\right)}, \quad (45)$$

or, by employing ,

$$A = \left(\frac{16-\pi^2}{2\pi}\right)^2 \left(\frac{N\pi^2}{16-\pi^2}\right)_2. \quad (46)$$

From (34), (40) can be equivalently expressed as

$$B = \mathbb{E}\left[\left(\kappa_t^2 + \kappa_r^2\right)|A|^2 + \frac{1}{\rho_s}\right], \quad (47)$$

which, according to [45], can be rewritten as

$$B = \left(\kappa_t^2 + \kappa_r^2\right)\mathbb{E}\left[|A|^2\right] + \frac{1}{\rho_s}, \quad (48)$$

or, with the aid of (33) and (39),

$$B = \left(\kappa_t^2 + \kappa_r^2\right)A + \frac{1}{\rho_s}. \quad (49)$$

By employing (46), (49) can be evaluated as

$$B = \left(\kappa_t^2 + \kappa_r^2\right)\left(\frac{16-\pi^2}{2\pi}\right)^2 \left(\frac{N\pi^2}{16-\pi^2}\right)_2 + \frac{1}{\rho_s}. \quad (50)$$

Finally, by substituting (46) and (50) into (38), we obtain (22). This concludes the proof.

### APPENDIX C PROOF OF LEMMA 1

From (22), the ergodic capacity ceiling can be obtained as in (51), given at the bottom of the page. Due to the fact that, as  $\rho_s$  tends to infinity,  $\frac{1}{\rho_s}$  tends to zero, (51) can be evaluated as in (23).

Similarly, for  $N$  tends to infinity, the ergodic capacity ceiling can be expressed as

$$C_N = \lim_{N \rightarrow \infty} C, \quad (52)$$

which, by employing (22) can be rewritten as

$$C_N = \lim_{N \rightarrow \infty} \left( \log_2 \left( 1 + \frac{\mathcal{K}(N)}{(\kappa_t^2 + \kappa_r^2)\mathcal{K}(N) + \frac{1}{\rho_s}} \right) \right), \quad (53)$$

where

$$\mathcal{K}(N) = \left(\frac{16-\pi^2}{2\pi}\right)^2 \left(\frac{N\pi^2}{16-\pi^2}\right)_2. \quad (54)$$

As  $N$  tends to infinity,  $\mathcal{K}(N)$  also tends to infinity. Therefore, by applying the de L' Hospital rule in (53) and after some algebraic manipulations, we extract (23). This concludes the proof.

$$\lim_{\rho_s \rightarrow \infty} C \leq \lim_{\rho_s \rightarrow \infty} \left( \log_2 \left( 1 + \frac{\left(\frac{16-\pi^2}{2\pi}\right)^2 \left(\frac{N\pi^2}{16-\pi^2}\right)_2}{(\kappa_t^2 + \kappa_r^2)\left(\frac{16-\pi^2}{2\pi}\right)^2 \left(\frac{N\pi^2}{16-\pi^2}\right)_2 + \frac{1}{\rho_s}} \right) \right) \quad (51)$$

## ACKNOWLEDGMENT

The authors would like to thank the Editor and anonymous reviewers for their constructive comments and criticism.

## REFERENCES

- [1] S. Dang, O. Amin, B. Shihada, and M.-S. Alouini, "What should 6G be?" *Nat. Electron.*, vol. 3, no. 1, pp. 20–29, Jan. 2020.
- [2] G. Gui, M. Liu, F. Tang, N. Kato, and F. Adachi, "6G: Opening new horizons for integration of comfort, security and intelligence," *IEEE Wireless Commun.*, early access, Mar. 03, 2020, doi: 10.1109/MWC.001.1900516.
- [3] M. di Renzo *et al.*, "Smart radio environments empowered by reconfigurable AI meta-surfaces: An idea whose time has come," *EURASIP J. Wireless Commun. Netw.*, vol. 2019, no. 1, pp. 1–20, May 2019.
- [4] L. Dai *et al.*, "Reconfigurable intelligent surface-based wireless communications: Antenna design, prototyping, and experimental results," *IEEE Access*, vol. 8, pp. 45913–45923, 2020.
- [5] C. Pan *et al.*, "Multicell MIMO communications relying on intelligent reflecting surfaces," *IEEE Trans. Wireless Commun.*, early access, May 08, 2020, doi: 10.1109/TWC.2020.2990766.
- [6] E. Basar, M. Di Renzo, J. De Rosny, M. Debbah, M. Alouini, and R. Zhang, "Wireless communications through reconfigurable intelligent surfaces," *IEEE Access*, vol. 7, pp. 116753–116773, 2019.
- [7] V. C. Thirumavalavan and T. S. Jayaraman, "BER analysis of reconfigurable intelligent surface assisted downlink power domain NOMA system," in *Proc. Int. Conf. Commun. Syst. Netw. (COMSNETS)*, Bengaluru, India, Jan. 2020, pp. 519–522.
- [8] H. Zhang, B. Di, L. Song, and Z. Han, "Reconfigurable intelligent surfaces assisted communications with limited phase shifts: How many phase shifts are enough?" *IEEE Trans. Veh. Technol.*, vol. 69, no. 4, pp. 4498–4502, Apr. 2020.
- [9] M. di Renzo *et al.*, "Reconfigurable intelligent surfaces vs. relaying: Differences, similarities, and performance comparison," *IEEE Open J. Commun. Soc.*, vol. 1, pp. 798–807, Jun. 2020.
- [10] E. Bjornson, O. Ozdogan, and E. G. Larsson, "Intelligent reflecting surface versus decode-and-forward: How large surfaces are needed to beat relaying?" *IEEE Wireless Commun. Lett.*, vol. 9, no. 2, pp. 244–248, Feb. 2020.
- [11] A.-A. A. Boulogeorgos and A. Alexiou, "Performance analysis of reconfigurable intelligent surface-assisted wireless systems and comparison with relaying," *IEEE Access*, vol. 8, pp. 94463–94483, 2020.
- [12] C. Huang, A. Zappone, G. C. Alexandropoulos, M. Debbah, and C. Yuen, "Reconfigurable intelligent surfaces for energy efficiency in wireless communication," *IEEE Trans. Wireless Commun.*, vol. 18, no. 8, pp. 4157–4170, Aug. 2019.
- [13] B. Di, H. Zhang, L. Song, Y. Li, Z. Han, and H. V. Poor, "Hybrid beamforming for reconfigurable intelligent surface based multi-user communications: Achievable rates with limited discrete phase shifts," *IEEE J. Sel. Areas Commun.*, early access, Jun. 08, 2020, doi: 10.1109/JSAC.2020.3000813.
- [14] S. Li, B. Duo, X. Yuan, Y.-C. Liang, and M. D. Renzo, "Reconfigurable intelligent surface assisted UAV communication: Joint trajectory design and passive beamforming," *IEEE Wireless Commun. Lett.*, vol. 9, no. 5, pp. 716–720, May 2020.
- [15] C. Pan *et al.*, "Intelligent reflecting surface aided MIMO broadcasting for simultaneous wireless information and power transfer," *IEEE J. Sel. Areas Commun.*, early access, Jun. 08, 2020, doi: 10.1109/JSAC.2020.3000802.
- [16] T. Schenk, *RF Imperfections in High-Rate Wireless Systems: Impact and Digital Compensation*. Dordrecht, The Netherlands: Springer, 2008. [Online]. Available: [https://www.ebook.de/de/product/11431698/tim\\_schenk\\_rf\\_imperfections\\_in\\_high\\_rate\\_wireless\\_systems.html](https://www.ebook.de/de/product/11431698/tim_schenk_rf_imperfections_in_high_rate_wireless_systems.html)
- [17] A.-A. A. Boulogeorgos, V. M. Kapinas, R. Schober, and G. K. Karagiannidis, "I/Q-imbalance self-interference coordination," *IEEE Trans. Wireless Commun.*, vol. 15, no. 6, pp. 4157–4170, Jun. 2016.
- [18] A.-A. A. Boulogeorgos, P. C. Sofotasios, B. Selim, S. Muhaidat, G. K. Karagiannidis, and M. Valkama, "Effects of RF impairments in communications over cascaded fading channels," *IEEE Trans. Veh. Technol.*, vol. 65, no. 11, pp. 8878–8894, Nov. 2016.
- [19] A.-A. A. Boulogeorgos, "Interference mitigation techniques in modern wireless communication systems," Ph.D. dissertation, Dept. Doctor Philos., Aristotle Univ. Thessaloniki, Thessaloniki, Greece, Sep. 2016.
- [20] A.-A. A. Boulogeorgos and G. K. Karagiannidis, "Energy detection in full-duplex systems with residual RF impairments over fading channels," *IEEE Wireless Commun. Lett.*, vol. 7, no. 2, pp. 246–249, Apr. 2018.
- [21] X. Yang, M. Matthaiou, J. Yang, C. Wen, F. Gao, and S. Jin, "Hardware-constrained millimeter-wave systems for 5G: Challenges, opportunities, and solutions," *IEEE Commun. Mag.*, vol. 57, no. 1, pp. 44–50, Jan. 2019.
- [22] E. Soleimani-Nasab, M. Matthaiou, M. Ardebilipour, and G. K. Karagiannidis, "Two-way AF relaying in the presence of co-channel interference," *IEEE Trans. Commun.*, vol. 61, no. 8, pp. 3156–3169, Aug. 2013.
- [23] L. Anttila, M. Valkama, and M. Renfors, "Circularity-based I/Q imbalance compensation in wideband direct-conversion receivers," *IEEE Trans. Veh. Commun.*, vol. 57, no. 4, pp. 2099–2113, Jul. 2008.
- [24] S. Zhou, W. Xu, K. Wang, M. Di Renzo, and M. Alouini, "Spectral and energy efficiency of IRS-assisted MISO communication with hardware impairments," *IEEE Wireless Commun. Lett.*, early access, Apr. 27, 2020, doi: 10.1109/LWC.2020.2990431.
- [25] Y. Liu, E. Liu, and R. Wang, "Energy efficiency analysis of intelligent reflecting surface system with hardware impairments," Apr. 2020. [Online]. Available: arXiv:2004.09804.
- [26] S. Hu, F. Rusek, and O. Edfors, "Capacity degradation with modeling hardware impairment in large intelligent surface," in *Proc. IEEE Global Commun. Conf. (GLOBECOM)*, Abu Dhabi, UAE, Dec. 2018, pp. 1–6.
- [27] J. V. Alegria and F. Rusek, "Achievable rate with correlated hardware impairments in large intelligent surfaces," in *Proc. IEEE 8th Int. Workshop Comput. Adv. Multi Sens. Adapt. Process. (CAMSAP)*, Le goser, Guadeloupe, Dec. 2019, pp. 559–563.
- [28] Z. Xing, R. Wang, J. Wu, and E. Liu, "Achievable rate analyses and phase shift optimizations on intelligent reflecting surface with hardware impairments," May 2020. [Online]. Available: arXiv:2005.14411.
- [29] I. S. Gradshteyn and I. M. Ryzhik, *Table of Integrals, Series, and Products*, 6th ed. San Diego, CA, USA: Academic, 2000.
- [30] H. Srivastava and J. Choi, *Introduction and Preliminaries*. Oxford, U.K.: Elsevier, 2011.
- [31] H. Holma and A. Toskala, *LTE for UMTS: Evolution to LTE-Advanced*, 2nd ed. Hoboken, NJ, USA: Wiley, Mar. 2011.
- [32] A.-A. A. Boulogeorgos, E. N. Pappasotiriou, and A. Alexiou, "Analytical performance assessment of THz wireless systems," *IEEE Access*, vol. 7, pp. 11436–11453, 2019.
- [33] S. Koenig *et al.*, "Wireless sub-THz communication system with high data rate," *Nat. Photon.*, vol. 7, pp. 977–981, Oct. 2013.
- [34] C. Studer, M. Wenk, and A. Burg, "MIMO transmission with residual transmit-RF impairments," in *Proc. Int. ITG Workshop Smart Antennas (WSA)*, Bremen, Germany, Feb. 2010, pp. 189–196.
- [35] M. Wenk, *MIMO-OFDM Testbed : Challenges, Implementations, and Measurement Results*(Series in Microelectronics). Konstanz, Germany: Hartung-Gorre, 2010.
- [36] B. E. Priyanto, T. B. Sorensen, O. K. Jensen, T. Larsen, T. Kolding, and P. Mogensen, "Assessing and modeling the effect of RF impairments on UTRA LTE uplink performance," in *Proc. IEEE 66th Veh. Technol. Conf.*, Baltimore, MD, USA, Sep. 2007, pp. 1213–1217.
- [37] E. Björnson, M. Matthaiou, and M. Debbah, "Massive MIMO systems with hardware-constrained base stations," in *Proc. IEEE Int. Conf. Acoust. Speech Signal Process. (ICASSP)*, Florence, Italy, May 2014, pp. 3142–3146.
- [38] E. Björnson, A. Papadogiannis, M. Matthaiou, and M. Debbah, "On the impact of transceiver impairments on AF relaying," in *Proc. IEEE Int. Conf. Acoust. Speech Signal Process. (ICASSP)*, Vancouver, BC, Canada, May 2013, pp. 4948–4952.
- [39] A.-A. A. Boulogeorgos, E. N. Pappasotiriou, and A. Alexiou, "Analytical performance evaluation of THz wireless fiber extenders," in *Proc. IEEE 30th Annu. Int. Symp. Pers. Indoor Mobile Radio Commun. (PIMRC)*, Istanbul, Turkey, Sep. 2019, pp. 1–6.
- [40] A.-A. A. Boulogeorgos, N. D. Chatzidiamentis, and G. K. Karagiannidis, "Energy detection spectrum sensing under RF imperfections," *IEEE Trans. Commun.*, vol. 64, no. 7, pp. 2754–2766, Jul. 2016.

- [41] V. S. Asadchy, M. Albooyeh, S. N. Tcvetkova, A. Díaz-Rubio, Y. Ra'di, and S. A. Tretyakov, "Perfect control of reflection and refraction using spatially dispersive metasurfaces," *Phys. Rev. B*, vol. 94, no. 7, Aug. 2016, Art. no. 075142.
- [42] X. Tan, Z. Sun, J. M. Jornet, and D. Pados, "Increasing indoor spectrum sharing capacity using smart reflect-array," in *Proc. IEEE Int. Conf. Commun. (ICC)*, Kuala Lumpur, Malaysia, May 2016, pp. 1–6.
- [43] S. G. Krantz, *Handbook of Complex Variables*. Boston, MA, USA: Springer, Oct. 1999.
- [44] E. Björnson, M. Matthaiou, and M. Debbah, "A new look at dual-hop relaying: Performance limits with hardware impairments," *IEEE Trans. Commun.*, vol. 61, no. 11, pp. 4512–4525, Nov. 2013.
- [45] J. J. Shynk, *Probability, Random Variables, and Random Processes: Theory and Signal Processing Applications*. Hoboken, NJ, USA: Wiley, 2013.



**ALEXANDROS-APOSTOLOS A. BOULOGEORGOS** (Senior Member, IEEE) was born in Trikala, Greece, in 1988. He received the Electrical and Computer Engineering (ECE) Diploma and Ph.D. degrees in wireless communications from the Aristotle University of Thessaloniki (AUTH) in 2012 and 2016, respectively.

From November 2012, he has been a Member of the Wireless Communications System Group, AUTH, working as a Research Assistant/Project Engineer in various telecommunication and networks projects. In 2017, he joined the Information Technologies Institute, while from November 2017, he has joined the Department of Digital Systems, University of Piraeus, where he conducts research in the area of wireless communications. From October 2012 until September 2016, he was a Teaching Assistant with the Department of ECE, AUTH, whereas, from February 2017, he serves as an Adjunct Lecturer with the Department of Informatics and Telecommunications Engineering, University of Western Macedonia and as a Visiting Lecturer with the Department of Computer Science and Biomedical Informatics, University of Thessaly. He has authored and coauthored more than 45 technical papers, which were published in scientific journals and presented at prestigious international conferences. Furthermore, he has submitted two (one national and one European) patents. His current research interests spans in the area of wireless communications and networks with emphasis in high frequency communications, optical wireless communications and communications for biomedical applications.

Dr. Boulogeorgos was awarded with the "Distinction Scholarship Award" of the Research Committee of AUTH for the year 2014 and was recognized as an exemplary reviewer for IEEE Communication Letters for 2016 (top 3% of reviewers). Likewise, he has been involved as member of Technical Program Committees in several IEEE and non-IEEE conferences and served as a reviewer in various IEEE journals and conferences. Moreover, he was named a top peer reviewer (top 1% of reviewers) in Cross-Field and Computer Science in the Global Peer Review Awards 2019, which was presented by the Web of Science and Publons. He is a member of the Technical Chamber of Greece.



**ANGELIKI ALEXIOU** (Member, IEEE) received the Diploma degree in electrical and computer engineering from the National Technical University of Athens in 1994 and the Ph.D. degree in electrical engineering from Imperial College of Science, Technology and Medicine, University of London in 2000. Since May 2009, she has been a Faculty Member with the Department of Digital Systems, University of Piraeus, where she conducts research and teaches undergraduate and postgraduate courses in the area of broad-

band communications and advanced wireless technologies. Prior to this appointment she was with Bell Laboratories, Wireless Research, Lucent Technologies, currently Alcatel-Lucent, Swindon, U.K., first as a Member of Technical Staff (January 1999 to February 2006) and later as a Technical Manager (March 2006 to April 2009). She is the Project Coordinator of the H2020 TERRANOVA project (ict-terranova.eu). Her current research interests include radio interface, MIMO and high frequencies (mmWave and THz wireless) technologies, cooperation, coordination and efficient resource management for ultra dense wireless networks and machine-to-machine communications, and 'cell-less' architectures based on softwarization, virtualization and extreme resources sharing. He is a co-recipient of Bell Labs President's Gold Award in 2002 for contributions to Bell Labs Layered Space-Time (BLAST) project and the Central Bell Labs Teamwork Award in 2004 for role model teamwork and technical achievements in the IST FITNESS project. He is the elected Chair of the Working Group on Radio Communication Technologies of the Wireless World Research Forum. She is a member of the IEEE and the Technical Chamber of Greece.